ChemPubSoc Europe

DOI: 10.1002/ejic.201701209

EurJIC European Journal of Inorganic Chemistry

Full Paper

Nitrogen Fixation

Coordination of 3-Methylindole-Based Tripodal Tetraphosphine Ligands to Iron(+II), Cobalt(+II), and Nickel(+II) and Investigations of their Subsequent Two-Electron Reduction

Fenna F. van de Watering,[a] Wowa Stroek,[a] Jarl Ivar van der Vlugt,[a] Bas de Bruin,[a] Wojciech I. Dzik,*[a] and Joost N. H. Reek*[a]

Abstract: We report the coordination chemistry of indole based tripodal tetraphosphine ligands to iron(II), cobalt(II) and nickel(II). These complexes are formed by simple synthetic protocols and were characterized by a combination of spectroscopic techniques and single-crystal X-ray analysis. The molecular structures as determined by X-ray diffraction show that the geometry of the nickel and cobalt complexes are distorted trigonal bipyramidal. The monocationic iron(II) complexes also have distorted trigonal bipyramidal geometries, but the dicationic analogue has an octahedral geometry. Two-electron reduction of the cobalt(+II) and the nickel(+II) complexes in the presence of N_2 did not lead to the coordination of N_2. In contrast, two-electron reduction of the iron(+II) complexes did lead to coordination of dinitrogen to the iron center. The Fe^0N_2**L1^H** complex has a trigonal bipyramidal geometry, and the N–N bond length of the coordinated dinitrogen ligand is longer than that of free dinitrogen, indicating that coordination to this iron(0) complex results in activation of the N≡N bond.

Introduction

Recent years brought about a renaissance of coordination chemistry of base metals. Their abundance and generally lower toxicity in comparison to noble metals makes them ideal candidates to explore them as new homogeneous catalysts.[1–4] Complexes of base metals with phosphine based ligands are among the many highly active catalysts that can facilitate very challenging reactions ranging from reduction of unsaturated compounds such as alkynes,[5] aldehydes[6] or carboxylic acids and esters[7] to reduction of CO_2.[8–14] In particular, expanding the coordination chemistry of base metals with tripodal, tetradentate ligands is attractive, as complexes of tripodal phosphine ligands with base metal iron and cobalt reveal outstanding activity in (among others) dehydrogenation/hydrogenation of CO_2-based fuels or reduction of N_2.[11,15–19]

We turned our attention to the tripodal, tetradentate tris[1-(diphenylphosphanyl)-3-methyl-1*H*-indol-2-yl]phosphane ligand (**L1^H**) (Figure 1), which has previously been used in coordination chemistry with Pd,[20] Rh,[21,22] Cu,[22] and Ru,[23,24] showing a remarkable potential to stabilize rare paramagnetic Rh^{II}[20] and Ru^I species,[23] as well as Ru^0 dinitrogen complexes.[23,24] These intriguing results triggered us to further explore the coordination behavior of the tripodal indolyl-based ligands with the earth abundant metals iron, cobalt and nickel. Tripodal tetradentate phosphine based complexes using either PP^{Ph}_3 = $P(CH_2CH_2PPh_2)_3$ or PP^{iPr}_3 = $[P(CH_2CH_2P^{iPr}_2)_3]$ coordinated to iron(+II), cobalt(+II) and nickel(+II) have been exten-

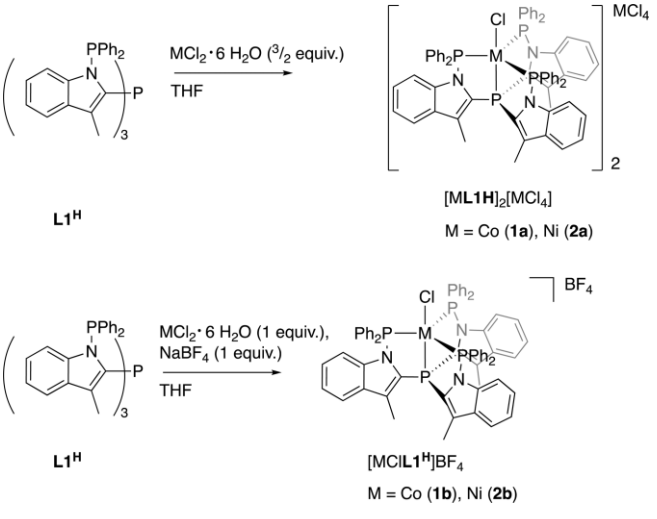

Figure 1. Coordination of cobalt(+II) and nickel(+II) chlorides to ligand **L1^H** forming the corresponding cobalt(+II) and nickel(+II) complexes **1** and **2**.

[a] *Homogeneous, Supramolecular and Bio-Inspired Catalysis, Van 't Hoff Institute for Molecular Sciences, University of Amsterdam, Science Park 904, 1098 XH, Amsterdam, The Netherlands*
E-mail: J.N.H.Reek@uva.nl
wdzik@wp.pl
http://www.uva.nl/en/profile/r/e/j.n.h.reek/j.n.h.reek.html
Supporting information and ORCID(s) from the author(s) for this article are available on the WWW under https://doi.org/10.1002/ejic.201701209.

sively studied.[25–30] These tripodal ligands generally occupy four coordination sites around a metal center and a trigonal bipyramidal geometry (TBP) is the most commonly observed geometry when the ligand is coordinated to a first row transition metal center.[29,31] These $[MX(PP_3)]^+$ complexes are formed by reacting the corresponding MX_2 salt with the ligand in the presence of a non-coordinating anion and can subsequently be reduced leading to the coordination of dinitrogen to the metal center.

In this paper, we first discuss the coordination of tripodal indolyl-based tetraphosphine ligands to the first-row late transition metals iron, cobalt, and nickel. The coordination of tris[1-(diphenylphosphanyl)-3-methyl-1*H*-indol-2-yl]phosphane (**L1^H**) to these metals is investigated in detail. Single crystal X-ray structure determination of these complexes allowed to study the changes in the coordination geometry of the ligand while stepwise increasing the d-electron count from d^6 to d^7 to d^8 by going from iron(+II) to cobalt(+II) to nickel(+II). Additionally, coordination studies of a variety of 3-methylindole based ligands ($L1^R$, $L2^H$ and $L3^{iPr}$) to iron(+II) and the synthetic challenges involved during coordination of these ligands to iron are reported.

In the second section, the electrochemical and chemical reduction of the above-mentioned complexes is described. Electrochemical reduction is used to evaluate if these complexes are redox-active. We further investigate the capability of these complexes to bind N_2 upon two-electron reduction with KC_8. In addition, we explored whether ligand modification leads to observable electronic effects in the N≡N stretch frequency when the PP_3 ligand is coordinated to iron. Additionally, the changes in the coordination geometry of the iron complexes upon reduction are discussed based on the crystal structures of iron(+I) complexes with ligands **L1^H**, **L2^H** and **L3^{iPr}** and iron(0) with ligand **L1^H**.

Results and Discussion

Formation of Mono and Binary Cobalt L1^H Complexes

We started our investigations with coordination studies of the tripodal indolyl-based tetraphosphine ligand (**L1^H**) to cobalt(+II). Mixing of stoichiometric amounts of **L1^H** and $CoCl_2{\cdot}6H_2O$ in THF did not lead to full consumption of **L1^H** as judged by in situ ^{31}P NMR spectroscopy. Cold Spray Electron Spray Ionization Mass Spectroscopy (CS-ESI-MS) revealed the presence of $CoCl_4^{2-}$ dianion which pointed to the possibility of the formation of a pentacoordinate $[Co(Cl)\mathbf{L1^H}]_2[CoCl_4]$ (**1a**) complex in which a part of the $CoCl_2$ acts as a chloride scavenger. Formation of tetrachlorido metallates upon coordination of multidentate ligands has been reported for several systems.[32–39] Therefore, we reacted **L1^H** with $CoCl_2$ in a 2:3 stoichiometry to quantitatively form the binary $[Co(Cl)\mathbf{L1^H}]_2[CoCl_4]$ complex **1a**. The monometallic complex could be obtained when the reaction was carried out in the presence of $NaBF_4$ (Figure 1) with the sodium cation acting as the scavenger of one of the chloride anions. This led to clean formation of $[Co\mathbf{L1^H}]BF_4$ (**1b**) from stoichiometric amounts of **L1^H** and $CoCl_2{\cdot}6H_2O$ in THF.

CS-ESI mass spectroscopy analysis showed the presence of the $[Co(Cl)\mathbf{L1^H}]^+$ cation in both $[Co(Cl)\mathbf{L1^H}]BF_4$ (**1b**) and $[Co(Cl)\mathbf{L1^H}]_2[CoCl_4]$ (**1a**) samples (see experimental section). Similar to findings reported by Braunstein and co-workers the $[Co(Cl)\mathbf{L1^H}]_2[CoCl_3]^+$ fragment could be detected in the $[Co(Cl)\mathbf{L1^H}]_2[CoCl_4]$ sample, indicating formation of the proposed binary complex.[29,40] Both the cationic and anionic cobalt complexes are paramagnetic. EPR analysis of the $[Co\mathbf{L1^H}]BF_4$ (**1b**) and $[Co(Cl)\mathbf{L1^H}]_2[CoCl_4]$ (**1a**) complexes in THF at 20 K are indicative for an $S = 1/2$ system with the cobalt(+II) ion being in a low-spin configuration (Figure 2). Small hyperfine couplings (presumably with cobalt and the phosphine atoms) are also noticeable In addition, the spectrum of $[Co(Cl)\mathbf{L1^H}]_2[CoCl_4]$ shows an extra signal (700–2500 G) corresponding to the high spin tetrachlorido cobaltate anion, which is absent in the $[Co\mathbf{L1^H}]BF_4$.

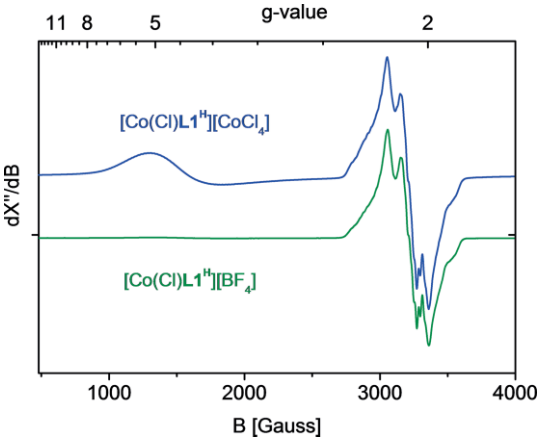

Figure 2. EPR spectra of $[Co(Cl)\mathbf{L1^H}]BF_4$ (green line) and $[Co(Cl)\mathbf{L1^H}]_2[CoCl_4]$ (blue line) measured in frozen THF at 20 K (Bu_4NPF_6 was added to obtain a better glass). Experimental parameters: microwave frequency 9.389 GHz, microwave power 0.632 mW, modulation amplitude 4 G.

Layering a dichloromethane solution of $[Co(Cl)\mathbf{L1^H}]_2[CoCl_4]$ with pentane resulted in the formation of single crystals suitable for X-ray diffraction analysis (Figure 3). As expected, the binary complex $[Co(Cl)\mathbf{L1^H}]_2[CoCl_4]$ **1a** is present in the crystal structure. The two $[Co(Cl)\mathbf{L1^H}]^+$ units crystallize as two independent molecules, which possess a very distorted geometry around the metal center, almost in-between a trigonal bipyramidal and square pyramidal geometry ($\tau_{5\#1} = 0.55$ and $\tau_{5\#2} = 0.67$)[41] (Table 1). This distortion is a result of the Jahn–Teller effect in combination with the rigidity of the backbone, which was also observed for the rhodium(+II) complex $[RhCl\mathbf{L1^H}]PF_6$ ($\tau_5 = 0.55$).[20] The four strong-field phosphine ligands favor the formation of low spin complexes, thus, d^7 complexes tend to form square pyramidal geometries. As the rigidity of the ligand scaffold does not allow such arrangement, a geometry in-between trigonal bipyramid and a square pyramid is formed. This is different for the iron(+II) and nickel(+II) analogues (vide infra) as these complexes possess intermediate spin d^6 or low spin d^8 metals, respectively and thus have a preference for the trigonal bipyramidal geometry with this ligand scaffold.

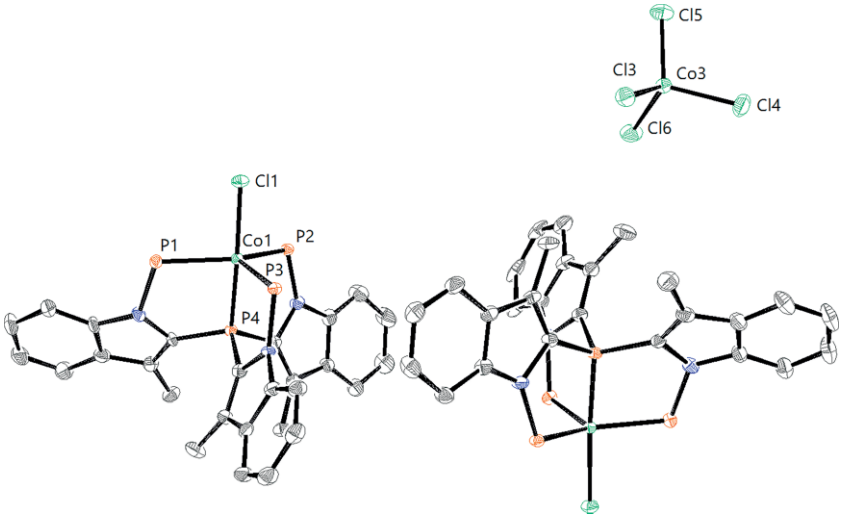

Figure 3. Displacement ellipsoid plot of [Co(Cl)**L1^{H}**]$_2$[$CoCl_4$] (**1a**) (50 % probability ellipsoids) (CCDC 1579207). Dichloromethane solvent molecules, phenyl rings and hydrogen atoms have been omitted for clarity.

Table 1. Selected bond lengths and angles of the [Co(Cl)**L1^{H}**]$_2$[$CoCl_4$] (**1a**) and [Ni(Cl)**L1^{H}**]$_2$[$NiCl_4$] (**2a**) complexes.

	[Co(Cl)**L1^{H}**]$_2$[$CoCl_4$] (**1a**) [Co(Cl)**L1^{H}**]$^+$ #1	[Co(Cl)**L1^{H}**]$^+$ #2	[Ni(Cl)**L1^{H}**]$_2$[$NiCl_4$] (**2a**) [Ni(Cl)**L1^{H}**]$^+$ #1	[Ni(Cl)**L1^{H}**]$^+$ #2
M1–P1	2.2422(11)	2.2691(11)	2.2187(10)	2.2562(10)
M1–P2	2.2590(11)	2.2652(11)	2.2435(10)	2.2548(10)
M1–P3	2.2673(11)	2.2550(11)	2.3108(10)	2.2772(10)
M1–P4	2.1432(11)	2.1434(11)	2.1321(10)	2.1290(10)
M1–Cl1	2.2401(11)	2.2382(11)	2.2345(10)	2.2323(10)
P1–M1–P2	140.74(4)	137.07(4)	131.39(4)	126.51(4)
P1–M1–P3	110.35(4)	109.62(4)	116.25(4)	116.47(4)
P2–M1–P3	107.23(4)	111.72(4)	111.39(4)	116.06(4)
P1–M1–P4	85.89(4)	85.26(4)	86.56(4)	86.74(4)
P2–M1–P4	85.28(4)	86.23(4)	86.30(4)	86.34(4)
P3–M1–P4	86.71(4)	86.38(4)	87.54(4)	87.23(4)
Cl1–M1–P4	173.63(5)	177.33(4)	173.23(4)	177.94(4)

Formation of Mono and Binary Nickel L1^{H} Complexes

Similar to the cobalt system, the coordination of nickel(+II) chloride hexahydrate to **L1^{H}** resulted in the formation of either the [Ni(Cl)**L1^{H}**]$_2$[$NiCl_4$] (**2a**) or the [Ni(Cl)**L1^{H}**]BF_4 (**2b**) complexes, depending on the use of $NaBF_4$ during the synthesis (Figure 1). As expected for the pentacoordinate d^8 complexes with strong-field phosphorus ligands, the [Ni(Cl)**L1^{H}**]$^+$ cations are diamagnetic, and thus NMR analysis of the complexes was possible. The identical ^{31}P NMR spectra of Ni(Cl)**L1^{H}**BF_4 (**1b**) and [Ni(Cl)**L1^{H}**]$_2$[$NiCl_4$] (**1a**) show one doublet (δ = 61.06 ppm) and one quartet (δ = 25.91 ppm), indicating a C_3-symmetrical trigonal bipyramidal geometry in solution (on the NMR time scale). C_3-symmetrical diamagnetic complexes of tripodal tetradentate phosphines coordinated to nickel have been previously reported,[29,42,43] and trigonal bipyramidal geometry was also reported for the d^8 [Ru(N_2)**L1^{H}**][23] and the [Pd(Cl)**L1^{H}**][Cl][22] complexes. Interestingly, whereas the coordination of nickel to **L1^{H}** results in the formation of the binary [Ni(Cl)**L1^{H}**]$_2$[$NiCl_4$] complex **2a**, the palladium complex does not form the tetrachlorido palladate, but one of the chloride anions remains non-coordinating.[20] In accordance with the NMR spectroscopic data, CSI mass spectrometry analysis showed the presence of the

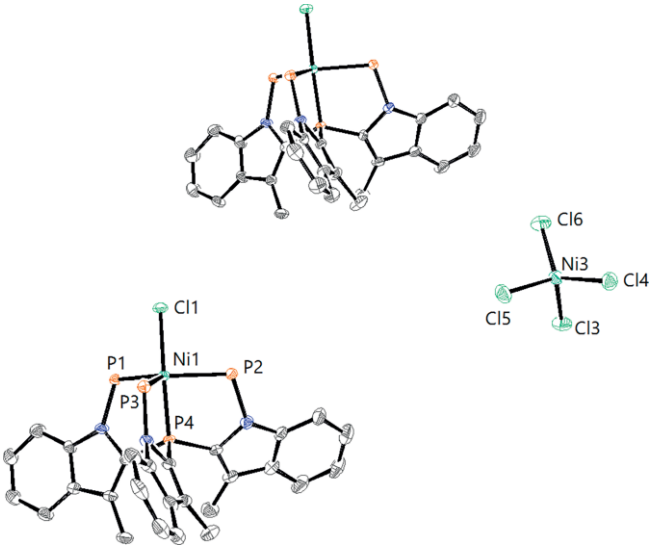

Figure 4. Displacement ellipsoid plot of [Ni(Cl)L1^{H}]$_2$[$NiCl_4$] (**2a**) (50 % probability ellipsoids) (CCDC 1579208). Dichloromethane solvent molecules, phenyl rings and hydrogen atoms have been omitted for clarity.

[Ni(Cl)**L1^{H}**]$^{+}$ ion in both [Ni(Cl)**L1^{H}**]BF_4 (**2b**) and [Ni(Cl)**L1^{H}**]$_2$-[$NiCl_4$] (**2a**) (see experimental section). Slow diffusion of hexane to a dichloromethane solution of [Ni(Cl)**L1^{H}**]$_2$[$NiCl_4$] resulted in the formation of crystals suitable for X-ray diffraction analysis (Figure 4).

The crystal structure shows the presence of the binary [Ni(Cl)**L1^{H}**]$_2$[$NiCl_4$] complex **2a** where the two [Ni(Cl)**L1^{H}**]$^{+}$ units crystallize as two independent molecules. The [Ni(Cl)**L1^{H}**]$^{+}$ units feature a distorted trigonal bipyramidal geometry around the metal center ($\tau_{5\#1}$ = 0.70 and $\tau_{5\#2}$ = 0.86) (Table 1).[41] The geometry is less distorted than the geometry of the cobalt analogues (vide supra), but more distorted than the geometry of the iron analogue, which is likely a result of the smaller atomic radius of the nickel atom compared to iron (vide infra). The largest angle P1–Ni–P2 is 131.39(4)° for one of the independent structures and 126.51(4)° for the other, which is still close to the ideal 120° angle for the TBP geometry.

Formation of Iron PP_3 Complexes

The above results show that the coordination of the tetradentate indolyl phosphine ligand **L1^{H}** to d^8 nickel(+II) and d^7 cobalt(+II) chlorides results in formation of (highly distorted in the case of cobalt) trigonal bipyramidal complexes of the type [M^{II}(Cl)**L1^{H}**]$^{+}$ and that in the absence of non-coordinating BF_4^- anion, binary tetrachlorido metallate complexes are formed. We next turned our attention to iron, and the results of these investigations are described in the following section. Whereas in the case of nickel and cobalt the **L1^{H}** ligand complexes are pentacoordinate, complexation of this ligand to d^6 iron(+II) could in principle result in formation of a hexacoordinate 18 VE complex, as was observed for iron's heavier analogue ruthenium,[23,24] or alternatively in the formation of a pentacoordinate 16 VE complex. Thus, we decided to study the coordination chemistry of iron in more detail, including the use of other tripodal indolyl phosphine ligands. The reaction of $FeCl_2$ with **L1^{H}** and $NaBF_4$ in THF in a 1:1:1 stoichiometry led to full conversion of the ligand according to the absence of its ^{31}P NMR signal, and the formation of a purple, paramagnetic complex as judged by the presence of broad peaks in the ^{1}H NMR spectrum in the region between 16.3 and 9.1 ppm. The paramagnetic behavior hinted at the formation of a five-coordinate species. CS-ESI mass spectrometry analysis in both positive and negative modes shows the presence of both the [Fe(Cl)**L1^{H}**]$^{+}$ complex and the BF_4^- counterion respectively, which is in accordance with a five-coordinate geometry around the metal center, supported by one non-coordinating anion. These data thus indicate that the synthesized compound is a pentacoordinate iron complex [Fe(Cl)**L1^{H}**]BF_4 (**3b**). DFT calculations suggest that the lowest energy state of the [Fe(Cl)**L1^{H}**]$^{+}$ cation is an intermediate spin, paramagnetic trigonal bipyramidal complex.[44] Iron(+II) (d^6) complexes with TBP geometry that are paramagnetic are not uncommon.[19,28,30,45,46] Crystals suitable for X-ray diffraction were obtained by layering a dichloromethane solution of [Fe(Cl)**L1^{H}**]BF_4 (**3b**) with pentane.

As anticipated, the crystal structure shows a trigonal bipyramidal geometry around the metal center (Figure 5). The overall crystal structural data is in good agreement with other tripodal five-coordinate tetraphosphine TBP iron(+II) complexes.[10,11,19,28,37,46] The longest equatorial angle P1–Fe1–P2 of 120.51(4)° (Table 2) fits well with that of an ideal TBP geometry, which is in correspondence with a τ_5 = 0.92.[41]

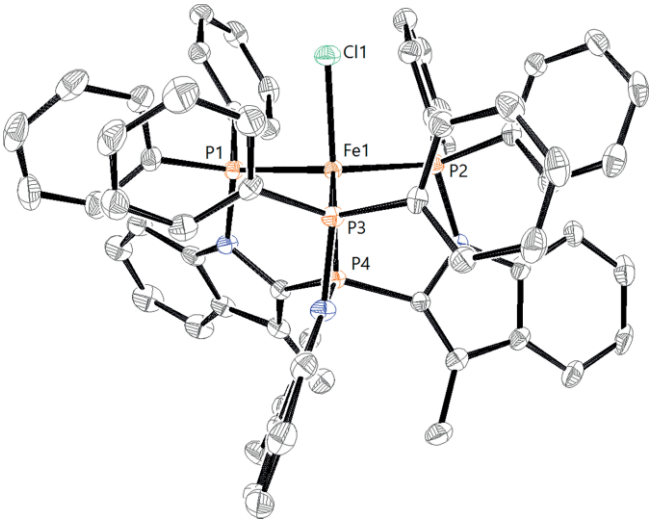

Figure 5. Displacement ellipsoid plot of [Fe(Cl)**L1^{H}**]BF_4 (**3b**) (50 % probability ellipsoids) (CCDC 1579209). Dichloromethane solvent molecule and hydrogen atoms and the BF_4^- counterion have been omitted for clarity.

Table 2. Selected bond lengths and angles of the [Fe(Cl)**L1^{H}**]BF_4 and [Fe(Cl)**L3^{iPr}**]$_2$[$FeCl_4$]$_2$ complexes.

	[Fe(Cl)**L1^{H}**]BF_4 (**3b**)	[Fe(Cl)**L3^{iPr}**]$_2$[$FeCl_4$]$_2$ (**7**)	
	[Fe(Cl)**L1^{H}**]$^{+}$	[Fe(Cl)**L3^{iPr}**]$^{+}$ #1	[Fe(Cl)**L3^{iPr}**]$^{+}$ #2
M1–P1	2.2721(9)	2.3542(11)	2.3762(12)
M1–P2	2.2765(10)	2.3851(11)	2.3975(12)
M1–P3	2.2748(9)	2.4021(12)	2.3710(12)
M1–P4	2.1952(8)	2.1729(11)	2.1711(11)
M1–Cl1	2.2145(8)	2.2136(11)	2.2070(12)
P1–M1–P2	120.51(4)	120.56(4)	120.23(4)
P1–M1–P3	118.37(3)	116.23(4)	117.95(4)
P2–M1–P3	117.52(4)	117.63(4)	116.26(4)
P1–M1–P4	83.36(3)	82.56(4)	82.01(4)
P2–M1–P4	83.96(3)	81.84(4)	81.70(4)
P3–M1–P4	83.70(3)	81.91(4)	82.64(4)
Cl1–M1–P4	178.58(4)	177.63(5)	178.95(5)

Subsequently, we explored the coordination of $FeCl_2$ to the PP_3 ligands **L1^{CF3}**, **L1^{OMe}**, **L2^{H}**, and **L3^{iPr}** in the presence of $NaBF_4$ (Figure 6) to form complexes **4**, **5**, **6**, and **7**, respectively. The new ligand **L3^{iPr}** was prepared by reacting the lithium salt of tris-2-(3-methylindolyl)phosphine[47] with diisopropyl chlorophosphine. Coordination of ligands other than **L1^{H}** to iron in presence of $NaBF_4$ did not provide the monometallic complex [Fe(Cl)**L**]BF_4 quantitatively as indicated by the presence of free ligand in the filtrate in the ^{31}P NMR spectrum. The addition of excess $NaBF_4$ to the purple to pink reaction mixtures nor the addition of alcohol as a co-solvent increases the yields of the product significantly.[19,27,46] Nevertheless, the CS-ESI mass spectrometry analysis of these reaction mixtures in the positive mode shows the presence of the [Fe(Cl)**L**]$^{+}$ cation, which indicates that the ligand does coordinate to the iron center. Analy-

sis in the negative mode showed the presence of the expected BF_4^- anion but also the presence of the $FeCl_3^-$ and $FeCl_4^-$ anions. These tetrachlorido ferrates are likely formed from the iron precursor, as was observed for the cobalt and nickel analogues, which is the reason that the reactions do not go to full conversion. When the purple reaction mixture from the reaction of **L3^{iPr}** with $FeCl_2$ in the presence of $NaBF_4$ was dissolved in dichloromethane and layered with pentane, crystals suitable for X-ray diffraction analysis formed. The crystal structure indeed contains the (oxidized) tetrachlorido ferrate anion $[FeCl_4]^-$ (likely formed in situ by a reaction of $[FeCl_4]^{2-}$ with traces of oxygen) as counterion, resulting in the binary [Fe(Cl)**L3^{iPr}**][$FeCl_4$] complex **7** (Figure 7).

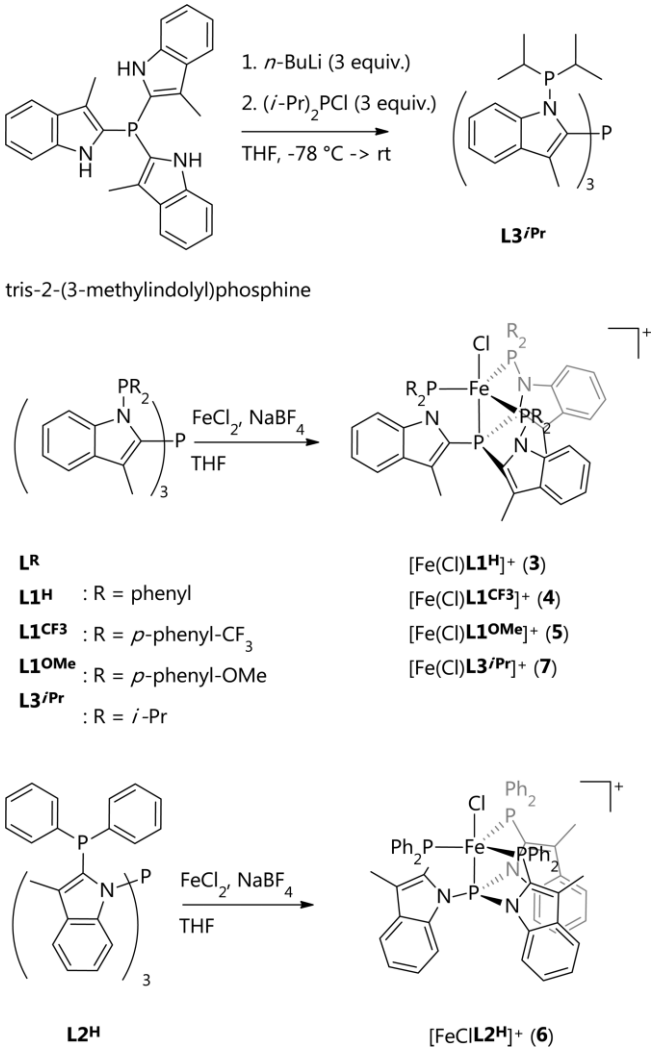

Figure 6. Synthesis of **L3^{iPr}** and coordination of **L1^{CF3}**, **L1^{OMe}**, **L3^{iPr}** and **L2^{H}** to $FeCl_2$ in the presence of $NaBF_4$.

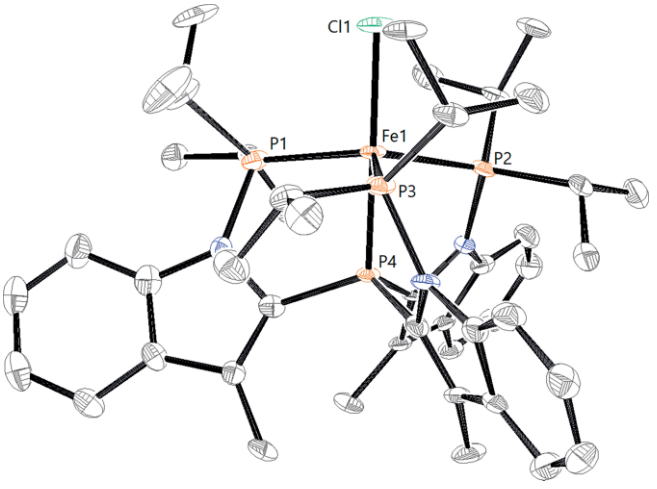

Figure 7. Displacement ellipsoid plot of [Fe(Cl)**L3^{iPr}**][$FeCl_4$] (**7**) (50 % probability ellipsoids) (CCDC 1579210). Hydrogen atoms and the $FeCl_4^-$ counterion have been omitted for clarity. The crystal of [Fe(Cl)**L3^{iPr}**][$FeCl_4$] reveals the presence of two independent $[Fe(Cl)\mathbf{L3}^{iPr}]^+$ cations and two independent $[FeCl_4]^-$ anions in the asymmetric unit.

[Fe(Cl)**L3^{iPr}**][$FeCl_4$] (**7**) crystallizes as two independent molecules (next to the tetrachlorido ferrate) with almost identical bond angles and distances. They both have a trigonal bipyramidal geometry ($\tau_{5\#1}$ = 0.95 and $\tau_{5\#2}$ = 0.98) (Table 1).[41] The P1–Fe1, P2–Fe1 and P3–Fe1 bond lengths are elongated compared to the $[Fe(Cl)\mathbf{L1}^{H}]^+$ unit, which is likely a result of the more electron-donating diisopropylphosphine groups. The other angles and distances are comparable to the $[Fe(Cl)\mathbf{L1}^{H}]^+$ unit and values reported in literature.[19,28,46]

The presence of tetrachlorido ferrates as counterions is undesired as iron chlorides could interfere during the follow-up redox chemistry. Therefore, a method previously described by Beller was used[11] that involved the coordination of **L1^{H}** to $Fe(BF_4)_2$ (Figure 8).

Stirring of stoichiometric amounts of **L1^{H}** and $Fe(BF_4)_2$ in 1:1 (v/v) THF/toluene mixture at 70 °C for three days led to precipi-

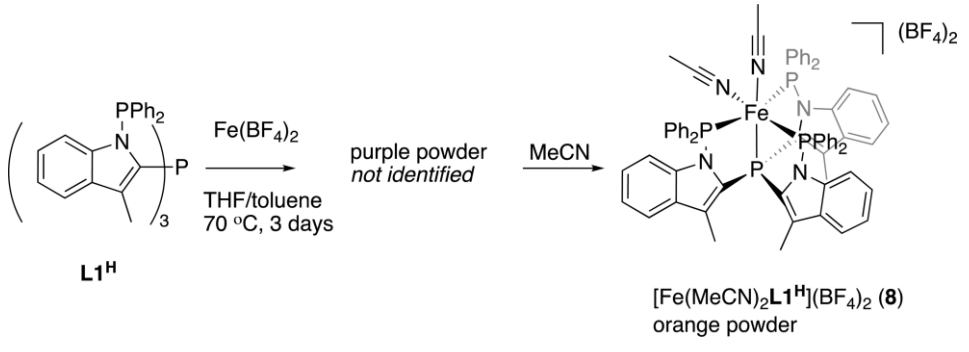

Figure 8. Complexation of $Fe(BF_4)_2$ with **L1^{H}**.

tation of a purple powder in significant amounts. Full conversion was, however, not reached as indicated by the presence of free ligand in the ^{31}P NMR spectrum of the supernatant. The exact structure of this highly oxygen sensitive purple solid could not be determined due to its paramagnetism and poor solubility in [D_8]THF. However, dissolution of the purple solid in acetonitrile caused an immediate color change from purple to orange. This orange solution was diamagnetic as evidenced by ^{31}P NMR spectroscopy, which indicates that the coordination environment around the metal center has changed. The ^{31}P NMR spectrum shows a similar splitting pattern as previously reported for the octahedral Ru(Cl)$_2$**L1^{H}** complex.[23] The integral-ratio of 1 (δ = 116.77 ppm, dt):2 (δ = 97.59 ppm, t):1 (δ = 56.18 ppm, dt) confirms formation of an octahedral geometry around the metal center. Crystals suitable for X-ray diffraction analysis were grown by slow diffusion of methanol to an acetonitrile solution of the orange iron complex. The crystal structure features two independent [Fe**L1^{H}**]$^{2+}$ units, which indeed show both an octahedral geometry around the metal center of the [Fe(MeCN)$_2$**L1^{H}**](BF$_4$)$_2$ complex **8** (Figure 9). The two *cis* sites in this complex are occupied by two acetonitrile ligands. The P1–Fe1–P2 [163.17(3)°], P3–Fe1–N4 [177.49(7)°], and the P4–Fe1–N5 angle [175.49(7)°] are all close to the theoretical 180° angle for an ideal octahedral geometry. The P1–Fe1 bond [2.3795(8) Å] is slightly longer than the other P_{eq}–Fe bonds [2.2576(8) Å and 2.2494(8) Å], and the axial acetonitrile ligand (N5–C66–C67), seems to bend in the direction of the P1–Fe1 bond.

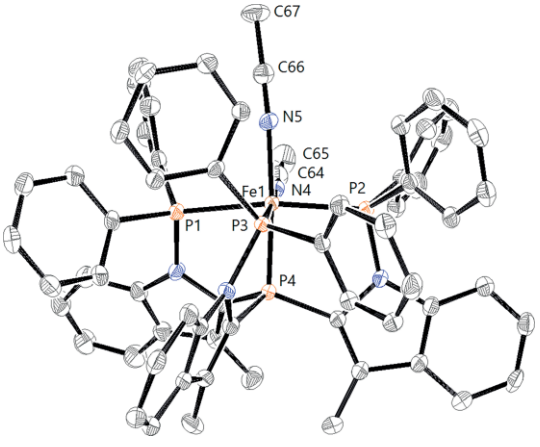

Figure 9. Displacement ellipsoid plot of [Fe**L1^{H}**(MeCN)$_2$](BF$_4$)$_2$ (**8**) (50 % probability ellipsoids) (CCDC 1579211). Methanol solvent molecules, hydrogen atoms and the BF_4^- counterions have been omitted for clarity. The crystal of [Fe**L1^{H}**(MeCN)$_2$]BF$_4$ reveals the presence of two independent [Fe**L1^{H}**-(MeCN)$_2$]$^{2+}$ dications and four independent BF_4^- anions in the asymmetric unit.

CS-ESI mass spectrometry analysis of an orange solution of the [Fe(MeCN)$_2$**L1^{H}**](BF$_4$)$_2$ complex in acetonitrile gave a clean mass spectrum, with major peaks for the [Fe(F)**L1^{H}**]$^+$ cation and the [Fe**L1^{H}**]$^{2+}$ di-cation. Most likely, the [Fe(F)**L1^{H}**]$^+$ is formed during the mass spectrometry experiment via a fluoride transfer reaction between the [Fe**L1^{H}**]$^{2+}$ di-cation and the BF_4^- anion. However, the formation of small amounts of [Fe(F)**L1^{H}**]BF$_4$ during coordination of **L1^{H}** to Fe(BF$_4$)$_2$ in a similar manner as reported by Beller and co-workers cannot be excluded.

Attempts to synthesize iron(+II) complexes with ligands **L1^{CF3}** and **L1^{OMe}**, provided only very low yield of the targeted compounds and therefore this method could unfortunately not be used for the coordination of iron to the other PP_3 ligands.

Reduction of the Cobalt, Nickel and Iron Complexes in Presence of N_2

Having the new iron, cobalt and nickel complexes in hand, we decided to investigate their reduction in the presence of dinitrogen. In analogy to ruthenium,[23,24] the iron complexes may bind N_2 upon two-electron reduction to form the respective pentacoordinate 18 VE iron(0) complexes. However, for the cobalt and nickel complexes the coordination of dinitrogen would likely require dissociation of one of the ligand arms for the complexes to adhere to the 18 VE rule. To evaluate whether the formation of dinitrogen complexes upon reduction of these complexes is possible, we conducted cyclic voltammetry (CV) studies and in situ reduction of the new complexes in the presence of N_2.

Reduction of [Co(Cl)L1^{H}]BF$_4$

In order to gain insight in the reduction potentials needed for the cobalt complexes to form the hypothetical Co^0**L1^{H}**N$_2$ complex, the [Co(Cl)**L1^{H}**]BF$_4$ (**1b**) complex was analyzed electrochemically. The CV of this cobalt complex shows one reversible redox couple ($E^0_{1/2}$ = –0.56 V vs. Fc/Fc$^+$), below which Co^{II} complex [Co(Cl)**L1^{H}**]BF$_4$ is reduced to Co^{I} complex [Co(Cl)**L1^{H}**] (see the Supporting Information). This value is slightly more negative than for the reversible Rh^{II}/Rh^{I} couple of the rhodium [Rh(Cl)**L1^{H}**]PF$_6$ analogue ($E^0_{1/2}$ = –0.4 V vs. Fc/Fc$^+$),[20] and comparable to the reversible Co^{II}/Co^{I} couple of the [Co(PP$^{Ph}_3$)-(CH$_3$CN)](BF$_4$)$_2$ complex ($E^0_{1/2}$ = –0.54 V).[48] Scanning to lower potentials resulted in two non-reversible reduction peaks at very similar potentials (E = –2.3 and –2.4 V vs. Fc/Fc$^+$). Likely, one of these peaks corresponds to the reduction of Co^{I} to Co^0, which could lead to binding of the dinitrogen to the cobalt center. Consequently, we also tried to reduce the [Co(Cl)**L1^{H}**]BF$_4$ (**1b**) complex chemically. The chemical reduction of the [Co(Cl)**L1^{H}**]BF$_4$ complex with 2 equiv. of KC$_8$ in the presence of N_2 was monitored by IR spectroscopy. The IR spectra did not show a signal corresponding to the dinitrogen stretch frequency typical for an N_2 coordination complex. In addition, in situ analysis of the reaction mixture by ^{31}P NMR spectroscopy showed signals indicative of ligand decomposition. Ligand decomposition may be responsible for the second reduction peak observed in the CV (E = –2.4 V vs. Fc/Fc$^+$). The inability of the complex to form N_2 coordinated complexes may be related to the strong coordination of the ligand, inhibiting the dissociation of one of the phosphine arms when it is bound to cobalt(0).

Reduction of [Ni(Cl)L1^{H}]BF$_4$

We also investigated the reduction potentials of the nickel complex using electrochemistry (see the Supporting Information).

Similar as for the cobalt analogue, the CV of **2b** shows one reversible reduction-oxidation peak at $E^0_{1/2}$ = –1.0 V vs. Fc/Fc$^+$ V. In addition, two non-reversible reduction peaks were observed (E = –2.0 V vs. Fc/Fc$^+$ and E = –2.5 V vs. Fc/Fc$^+$). CV measurements of [Ni(PP$^{Ph}_3$)(CH$_3$CN)](BF$_4$)$_2$ showed only one reversible redox couple ($E^0_{1/2}$ = –1.03 V vs. Fc/Fc$^+$; likely the Ni^{II}/Ni^I couple) and one non-reversible reduction peak, ($E^0_{1/2}$ = –1.28 V vs. Fc/Fc$^+$; likely the Ni^I/Ni^0 couple).[42,48] The chemical reduction of our [Ni**L1^H**]BF$_4$ (**2b**) complex with two equivalents of KC$_8$ resulted in formation of a yellow precipitate. Unfortunately, we were unable to measure ^{31}P NMR or infrared spectra of this yellow precipitate, as the complex is insoluble in both THF and benzene. The filtrate of the reaction mixture did not show any IR signal corresponding to an N$_2$ ligand bound to nickel. Comparable to the cobalt analogue, this result likely indicates that the ligand does not facilitate dinitrogen coordination when bound to nickel(0).

Reduction of [Fe(Cl)L1^H]BF$_4$

Next, we investigated whether it was possible to reduce the [Fe(Cl)**L1^H**]BF$_4$ (**3**) complex electrochemically. The cyclic voltammogram (see Figure S19) of [Fe(Cl)**L1^H**]BF$_4$ (**3**) in THF shows two reversible redox couples, one at $E^0_{1/2}$ = –0.38 V vs. Ag$^+$/AgCl (–0.96 V vs. Fc/Fc$^+$) and one at $E^0_{1/2}$ = –1.29 V vs. Ag/AgCl (–1.9 V vs. Fc/Fc$^+$), corresponding to the Fe^{III}/Fe^{II} and Fe^{II}/Fe^I couple respectively. The latter Fe^{II}/Fe^I reduction potential is much lower than the earlier mentioned paramagnetic [Fe(Cl)PP$^{Ph}_3$]$^+$ complex of Bianchini ($E^0_{1/2}$ = –0.64 V vs. Ag/AgCl).[30] Like Bianchini's complex, the reduction of Fe^I to Fe^0 likely takes place very close to the reduction wave of THF, and can therefore not be determined. From this data is was not apparent if we would be able to reduce the [Fe(Cl)**L1^H**]BF$_4$ (**3**) complex chemically and bind dinitrogen to the metal center. However, the addition of two equivalents of KC$_8$ in the presence of N$_2$ led to the formation of the Fe(N$_2$)**L1^H** (**9**) complex as indicated by the N$_2$ stretch frequency observed in the IR spectrum (Figure 10 and Table 3). Encouraged by this result we also attempted to reduce the other iron complexes with KC$_8$.

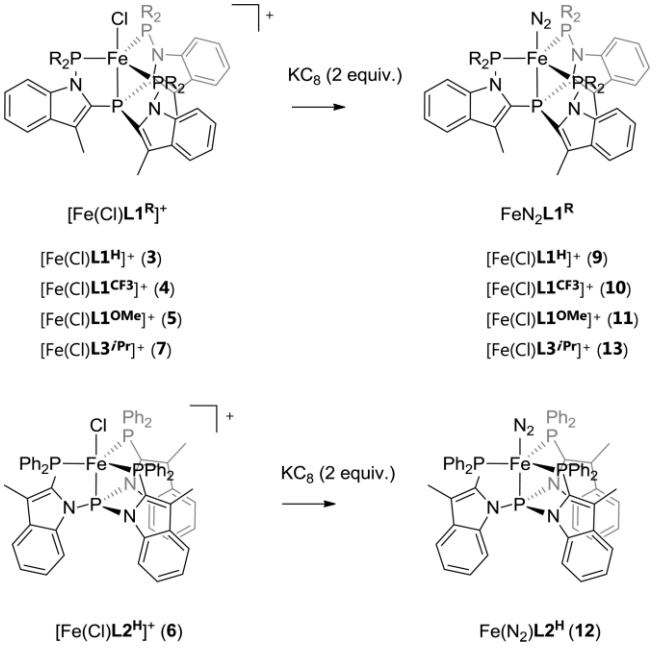

Figure 10. Two-electron reduction of iron(II) complexes with 3-methylindole-based tripodal tetraphosphine ligands in the presence of N$_2$.

Table 3. Reduction potentials of [M(Cl)**L1^H**]BF$_4$ complexes.

Complex	E^0 M^{III}/M^{II}	E^0 M^{II}/M^I
[Co(Cl)**L1^H**]BF$_4$ (**1b**)		–0.56 V
[Ni(Cl)**L1^H**]BF$_4$ (**2b**)		–1.00 V
[Fe(Cl)**L1^H**]BF$_4$ (**3**)	–0.96 V	–1.90 V

Reduction of Other Iron(+II)ClPP$_3$ Complexes

The in situ formed iron(0)N$_2$PP$_3$ complexes, prepared by two-electron reduction of the corresponding iron(+II) complexes with KC$_8$, all showed coordination of dinitrogen to the iron metal center as indicated by infrared spectroscopy measurements (Table 4). The Fe(N$_2$)**L2^H** complex **12** has the highest IR stretch frequency (ν_{N2} = 2068 cm^{-1}) and Fe(N$_2$)**L3^{iPr}** (**13**) has the lowest IR stretch frequency (ν_{N2} = 2018 cm^{-1}) in the infrared spectrum.

Table 4. N$_2$ stretch frequencies of the FeN$_2$**L** complexes.

Complex	ν_{N2} [cm^{-1}]
Fe(N$_2$)**L1^H** (**9**)	2055 and 2036
Fe(N$_2$)**L1^{CF3}** (**10**)	2051
Fe(N$_2$)**L1^{OMe}** (**11**)	2040 and 2026
Fe(N$_2$)**L2^H** (**12**)	2068
Fe(N$_2$)**L3^{iPr}** (**13**)	2018

As expected, the extent of activaton of N$_2$ by iron complexes with the 3-methylindole based tetraphosphine ligands **L1^H**, **L1^{CF3}**, **L1^{OMe}** and **L2^H** is higher than for the analogous ruthenium complexes.[24] The increase of the electron donating capacity of the substituents of the equatorially coordinated phosphines when going from **L1^{CF3}** to **L3^{iPr}** results in a clear shift of the N$_2$ stretch frequency to lower wavenumbers. The weakest activation of the N$_2$ ligand is observed in the case of the connectivity isomer **L2**, which features a more π-acidic pivotal phosphine (*trans* to the N$_2$). This is in line with the studies of the influence of π-acidity of the donors *trans* to molybdenum-coordinated N$_2$ by Tuczek et al. who reported that when going from purely σ-donating N-donor to a slightly π-acidic P-donor the N$_2$ stretch frequency shifts to higher wavenumbers.[49] The effect of the *trans*-effect of nitrogen vs. phosphorus in terms of N$_2$ activation is also apparent when comparing the IR data for Fe^0(N$_2$)[N(CH$_2$CH$_2$PPh$_2$)$_3$] ν_{N2} = 1967 cm^{-1} vs. Fe^0(N$_2$)-[P(CH$_2$CH$_2$P$^{iPr}_2$)$_3$] (ν_{N2} = 1985 cm^{-1}) as reported by the groups of George and Zubieta[50] and Field,[19] respectively.

Compared to the iron complexes with tripodal tetradentate ligands used by the group of Peters for N_2 reduction to ammonia or hydrazine,[51–53] the dinitrogen complexes reported in this work reveal higher stretch frequencies of the N_2 ligand. For instance, the dinitrogen complexes of iron(0) with ligands featuring three diisopropyl phosphine donors connected via a phenylene linker to the pivotal B, C^- and Si^- coordination centers $Fe^0(BP^{iPr}_3)N_2$,[52] $[Fe^0(CP^{iPr}_3)N_2]^-$,[53] $[Fe^0(SiP^{iPr}_3)N_2]^-$,[52] reveal ν_{N2} = 2011 cm^{-1}, 1870 cm^{-1} and 1891 cm^{-1} respectively. Since ligands CP^{iPr}_3 and SiP^{iPr}_3 are anionic, the extent of π-back donation to the N_2 moiety in their respective iron complexes is obviously higher than in the case of the **L3^{iPr}** complex. However, the overall donating capability of BP^{iPr}_3 (which is the most effective tripodal system for N_2 activation[15]) to iron is similar to **L3^{iPr}**. The major difference between BP^{iPr}_3 and the 3-methylindolyl-based ligand systems presented in this work is the capability of BP^{iPr}_3 to accommodate a negatively charged $[Fe^{-I}(N_2)\mathbf{L}]^-$ complex upon one electron reduction of the neutral $Fe(N_2)\mathbf{L}$, resulting in further weakening of the N–N bond (ν_{N2} = 1905 cm^{-1}), and rendering this complex an active catalyst for ammonia formation. The stabilization of such Fe^{-I} species is possible thanks to the incorporation of the σ-acidic boron atom in the BP^{iPr}_3 ligand. Unfortunately, the addition of one extra equivalent of KC_8 to $Fe^0(N_2)PP_3$ led to the detection of decomposed ligand in the ^{31}P NMR spectra. In addition, no new bands corresponding to the N_2 stretch frequency were detected in the infrared spectrum. The resulting reaction mixtures proved to be EPR silent. This led us to conclude that such putative negatively charged complexes are too unstable to be detected, or perhaps not formed at all.

All of the reaction mixtures that were prepared for the in situ analysis of the N_2 stretch frequency with infrared spectroscopy were set for crystallization by slow diffusion evaporation with pentane. In the case of Fe(Cl)**L1^H** (**14**), Fe(Cl)**L2^H** (**15**) and Fe(Cl)**L3^{iPr}** (**16**), crystals suitable for X-ray diffraction were obtained for some of these batches (Figure 11). In all three cases, analysis of the crystal structure showed the presence of the Fe^I(Cl)**L** complex, indicating that the reduction reactions intended to form Fe^0N_2**L** did not go to completion, and besides the desired iron(0) species also iron(+I) complexes are formed. As expected for a d^7 metal complexes, all three iron(+I) complexes feature a distorted trigonal bipyramidal geometry around the metal center due to the Jahn–Teller effect: Fe(Cl)**L1^H** (τ_5 = 0.75), Fe(Cl)**L2^H**(τ_5 = 0.69) and Fe(Cl)**L3^{iPr}** (τ_5 = 0.75) (Table 5).

Upon addition of a slight excess of KC_8 to the $[Fe(Cl)\mathbf{L1^H}]BF_4$ complex, a more intense absorption of the N_2 moiety was observed in the IR spectrum. When this red reaction mixture was set for crystallization by layering with pentane, crystals of $Fe(N_2)$**L1^H** (**9**) complex formed that were suitable for X-ray diffraction analysis (Figure 12). The crystal structure of $Fe(N_2)$**L1^H** reveals a nearly ideal trigonal bipyramidal geometry around the metal center (τ_5 = 0.95).[41] The structure is more symmetrical than the iron(+II) and ruthenium(0)[23] analogues, but structurally comparable to the known $Fe(N_2)(PP^{iPr}_3)$ (ν_{N2} = 1985 cm^{-1}) complex.[19] The N–N bond length of FeN_2**L1^H** is slightly shorter [1.118(5) Å] than in $FeN_2(PP^{iPr}_3)$ [1.1279(16) Å], which is in accordance with a less activated N_2 moiety in $Fe(N_2)$**L1^H**. These experiments therefore show that electronic variation in the ligands that coordinate to the iron metal have a clear effect on the activation of N_2 bound to Fe.

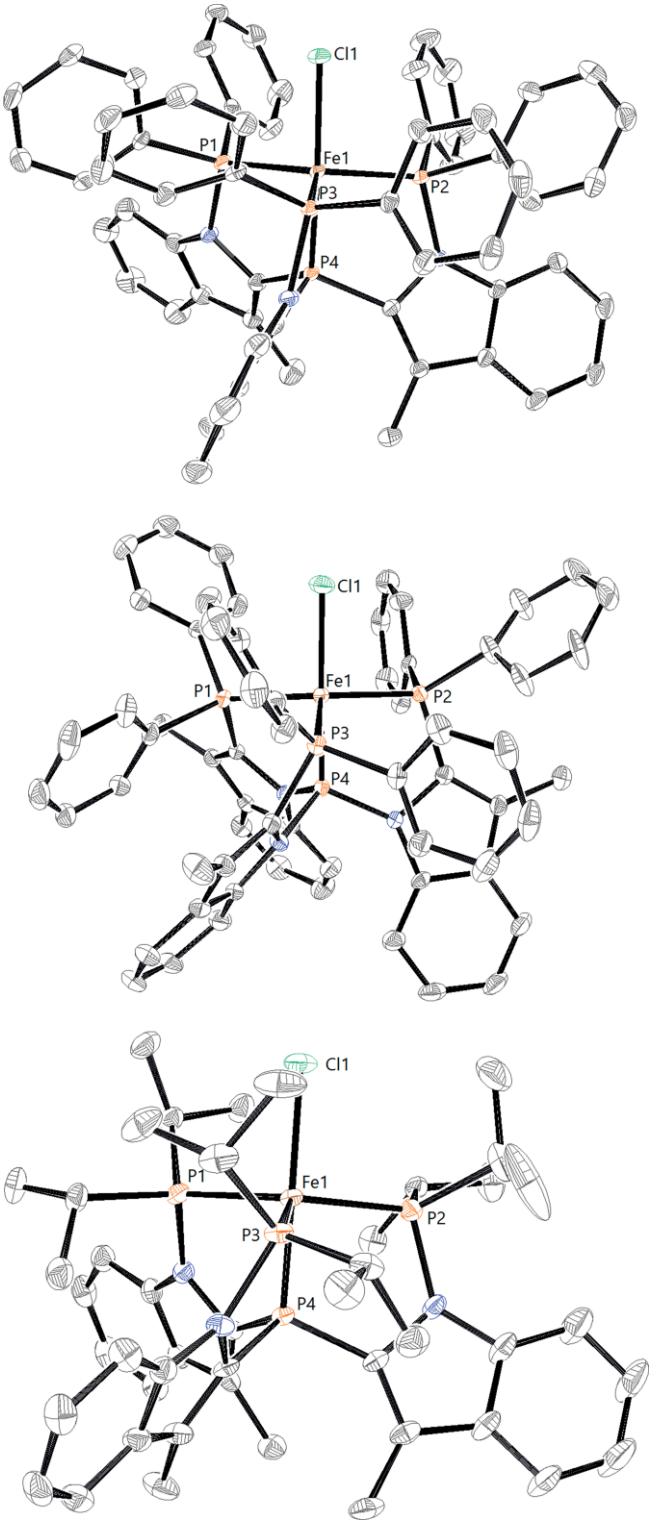

Figure 11. Displacement ellipsoid plot of [Fe(Cl)**L1^H**] (**14**) (top) (CCDC 1579212), [Fe(Cl)**L2^H**] (**15**) (middle) (CCDC 1579213) and [Fe(Cl)**L3^{iPr}**] (**16**) (bottom) (CCDC 1579214) (50 % probability ellipsoids). Solvent molecules and hydrogen atoms have been omitted for clarity.

Table 5. Selected bond lengths and angles of the FeCl**L1^{H}** (**14**), FeCl**L2^{H}** (**15**), FeCl**L3^{iPr}** (**16**) and FeN$_2$**L1^{H}** (**9**) complexes.

	Fe(Cl)**L1^{H}** (**14**)	Fe(Cl)**L2^{H}** (**15**)	Fe(Cl)**L3^{iPr}** (**16**)	Fe(N$_2$)**L1^{H}** (**9**)
Fe1–P1	2.2214(9)	2.2577(7)	2.3439(9)	2.1537(12)
Fe1–P2	2.2045(9)	2.2231(7)	2.2448(9)	2.1611(13)
Fe1–P3	2.1970(9)	2.2372(7)	2.2563(9)	2.1601(13)
Fe1–P4	2.1137(9)	2.0448(7)	2.0951(8)	2.1295(12)
Fe1–Cl1	2.3003(9)	2.2869(7)	2.3024(8)	
Fe1–N1				1.818(4)
N1–N2				1.118(5)
P1–Fe1–P2	131.87(4)	134.19(3)	130.12(3)	120.76(5)
P1–Fe1–P3	115.67(4)	109.11(3)	114.44(3)	116.69(5)
P2–Fe1–P3	110.52(3)	111.60(3)	112.53(3)	120.70(5)
P1–Fe1–P4	84.63(3)	80.81(3)	83.29(3)	85.87(5)
P2–Fe1–P4	86.00(3)	83.81(3)	85.25(3)	84.99(5)
P3–Fe1–P4	85.76(3)	83.45(3)	84.67(3)	85.59(5)
Cl1–Fe1–P4	177.15(4)	169.87(3)	175.37(4)	
N1–Fe1–P4				178.04(12)

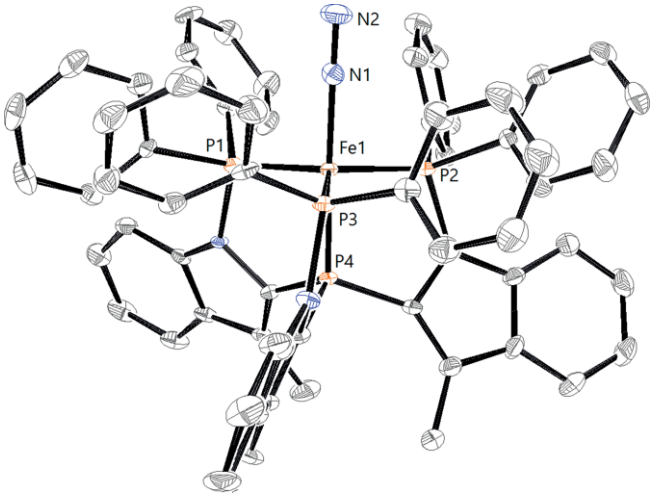

Figure 12. Displacement ellipsoid plot of FeN$_2$**L1^{H}** (**9**) (50 % probability ellipsoids) (CCDC 1579215). Hydrogen atoms and THF solvent molecule have been omitted for clarity.

Conclusions

In conclusion, we have shown that the coordination of iron(+II), cobalt(+II) and nickel(+II) to several tripodal 3-methylindole phosphine based ligands results in the formation of the corresponding cationic metal(+II) complexes. All of the complexes featuring the bulky chlorido ligand are five coordinate, with a non-coordinating counterion, which can be either BF_4^- or $[MCl_4]^{2-}$. In addition, one octahedral iron PP_3 complex was prepared, which features two acetonitrile ligands in *cis* position. The crystal structures obtained give clear insight in the coordination geometry around the metal centers, which is dependent on the number of d-electrons of the metal: a (distorted) trigonal bipyramidal geometry, where the cobalt complex is the most distorted as a result of the Jahn–Teller effect. The geometry of the nickel complex is more distorted than that of iron, which is likely a result of the smaller atomic radius of the nickel atom compared to iron atom. The two-electron reduction of the cobalt(+II) and the nickel(+II) complex in the presence of N_2 did not lead to the coordination of N_2. However, two-electron reduction of the iron(+II) complexes did lead to coordination of dinitrogen to the iron center. The corresponding iron-dinitrogen complexes, showed observable electronic effects in the N–N stretch frequency as a result of the ligand modifications: The complex Fe(N$_2$)**L2^{H}** featuring the most π-acidic phosphorus donor *trans* to the coordinated N_2 ligand has the highest IR stretch frequency (ν_{N2} = 2068 cm^{-1}) while introduction of strongly s-donating groups in complex Fe(N$_2$)**L3^{iPr}** resulted in the lowest IR stretch frequency (ν_{N2} = 2018 cm^{-1}) within the Fe(N$_2$)**L** series. The coordination of dinitrogen to the iron(0)PP_3 complexes is interesting in the light of the potential application of these complexes as dinitrogen reduction catalysts, as the coordination of dinitrogen to the metal is the first step in dinitrogen reduction to ammonia.

Experimental Section

General Methods: All reactions were carried out under an atmosphere of nitrogen using standard Schlenk techniques or in the glovebox. Reagents were purchased from commercial suppliers and used without further purification. THF, pentane, hexane and Et_2O were distilled from sodium benzophenone ketyl, CH_2Cl_2 was distilled from CaH_2 under nitrogen. NMR spectra [^{1}H, ^{31}P, and ^{13}C(^{1}H, ^{31}P)] were measured on a Bruker DRX 500, Bruker AV 400, Bruker DRX 300 or on a Bruker AV 300 spectrometer. IR spectra (ATR mode) were recorded with a Bruker Alpha-p FT-IR spectrometer. High resolution mass spectra were recorded on a JEOL AccuTOF LC, JMS-T100LP mass spectrometer using cold electron-spray ionization (CSI) at –40 °C. **L1^{H}**,[21] **L1^{CF3}**,[24] **L1^{OMe}**[24] and **L2^{H}**[22] were prepared in two steps from 3-methylindole. KC_8 was prepared by the method of Weitz and Rabinovitz.[54] Experimental X-band EPR spectra were recorded on a Bruker EMX spectrometer equipped with a He temperature control cryostat system (Oxford Instruments). Crystallographic data was obtained using a Bruker D8 Quest Eco diffractometer equipped with a Triumph monochromator and a Photon 50 detector. The intensities were integrated with the SAINT software package.[55] Multiscan absorption correction and scaling was performed with SADABS.[56] The structure was solved with Intrinsic Phasing Methods using SHELXT.[57] Least-squares refinement was performed with SHELXL 2013[58] against F^2 of all reflections. Non-hydrogen atoms were refined freely with anisotropic displacement parameters. All hydrogen atoms were located in difference Fourier maps and refined with a riding model. Structures of [Co(Cl)**L1^{H}**]$_2$[$CoCl_4$], [Ni(Cl)**L1^{H}**]$_2$[$NiCl_4$], [Fe(MeCN)$_2$**L1^{H}**]$(BF_4)_2$ and [Fe(Cl)**L3^{iPr}**]-

[$FeCl_4$] have solvent accessible voids filled with disordered solvent that could not be satisfactorily refined. Their contribution to the structure factors in the refinement was taken into account with the PLATON/SQUEEZE approach.[59]

Tris-2-(3-methyl-*N*-diisopropylphosphinoindolyl)phosphine (L3^{iPr}): Tris-2-(3-methylindolyl)phosphine (1.02 g; 2.42 mmol; 1.0 equiv.) was dissolved in THF (50 mL) and cooled to –78 °C. To this was added *n*BuLi (2.5 M in hexanes; 2.9 mL; 7.38 mmol; 3.0 equiv.) dropwise and stirred for 1 h resulting in a yellow solution. Subsequently, chlorodiisopropylphosphine (1.2 mL; 7.38 mmol; 3.0 equiv.) was added dropwise and the mixture was stirred for 3 d allowing the reaction mixture to warm to room temperature. The yellow solution was evaporated to dryness, and the thus formed solid was extracted with CH_2Cl_2 (3 × 10 mL). The combined CH_2Cl_2 solutions were filtered through basic alumina and evaporated in vacuo. The formed solid was washed with Et_2O (3 × 1 mL), yielding the product in pure form as a white powder (0.83 g; 45 % yield). $^1H\{^{31}P\}$ NMR (300 MHz, $CDCl_3$): δ = 7.51 (d, J = 16.4 Hz, 3 H), 7.49 (d, J = 15.8 Hz, 3 H), 7.21 (m, 6 H) 2.93–2.61 (m, 6 H), 1.90 (s, 9 H), 1.24 (d, J = 6.9 Hz, 9 H), 1.11 (d, J = 7.0 Hz, 9 H), 0.88 (d, J = 6.8 Hz, 9 H), 0.46 (d, J = 6.9 Hz, 9 H) ppm. ^{31}P NMR (121 MHz, $CDCl_3$): δ = 63.35 (d, J = 168.7 Hz, 3 P), –77.94 (q, J = 168.8 Hz, 1 P) ppm. $^{13}C\{^1H,^{31}P\}$ NMR (75 MHz, $CDCl_3$): δ = 140.90, 137.14, 133.30, 123.64, 122.19, 119.51, 118.95, 112.98, 27.19, 26.51, 21.85, 21.31, 20.18, 19.44, 10.03 ppm. Mass Analysis (CS-ESI) [**L3^{iPr}**]$^+$: found: 769.39843 calcd.: 769.39724.

[Co(Cl)L1^H]$_2$[CoCl$_4$] (1a): Compound **L1^H** (103.4 mg; 0.11 mmol; 2.0 equiv.) and $CoCl_2$·$6H_2O$ (43.6 mg; 0.16 mmol; 3.0 equiv.) were suspended in THF (10 mL) and stirred overnight. Pentane was added until all of the complex had precipitated. This brown solid was filtered off, washed with pentane and dried in vacuo yielding the complex as a brown solid. Yield: 108.4 mg (0.046 mmol, 87.4 %) Layering of a dichloromethane solution of [Co(Cl)**L1^H**]$_2$[$CoCl_4$] with pentane resulted in crystals suitable for X-ray diffraction analysis. Mass Analysis (CS-ESI) [Co(Cl)**L1^H**-H]$^+$: found: 1067.2092 calcd.: 1067.2054; ([Co(Cl)**L1^H**]$_2$[$CoCl_3$])$^+$: found: 2302.2782, calcd.: 2302.2511; [$CoCl_3$]$^-$: found: 163.8409, calcd.: 163.8398. EPR analysis of the complex was performed in THF at 20 K.

[Co(Cl)L1^H]BF$_4$ (1b): Compound **L1^H** (115.3 mg; 0.12 mmol; 1.0 equiv.), $NaBF_4$ (11.3 mg; 0.10 mmol; 1.0 equiv.) and $CoCl_2$·$6H_2O$ (113 mg; 0.12 mmol; 1.0 equiv.) were suspended in THF (10 mL) and stirred overnight. The brown precipitate was filtered off, washed with Et_2O and dried in vacuo yielding the complex as a brown solid. Yield: 110.3 mg (0.095 mmol, 92.8 %). Mass Analysis (CS-ESI) [Co(Cl)**L1^H**-H]$^+$: found: 1067.2092 calcd.: 1067.2054; BF_4^-: found: 87.0012, calcd.: 87.0029. EPR analysis of the complex was performed in THF at 20 K.

[Ni(Cl)L1^H]$_2$[NiCl$_4$] (2a): Compound **L1^H** (104.1 mg; 0.11 mmol; 1.0 equiv.) and $NiCl_2$·$6H_2O$ (38.2 mg; 0.16 mmol; 1.0 equiv.) were suspended in THF (10 mL) and stirred overnight. Pentane was added until all of the complex had precipitated. The green precipitate was filtered off, washed with Et_2O and was dried in vacuo yielding the complex as a green solid. Yield: 94.3 mg (0.041 mmol, 76.8 %). ^1H NMR (300 MHz, $CDCl_3$): δ = 7.81 (d, J = 8.1 Hz, 3 H), 7.27–7.17 (m, 9 H), 7.12–6.82 (m, 29 H), 6.29 (d, J = 8.5 Hz, 3 H), 2.67 (s, 9 H) ppm. ^{31}P NMR (121 MHz, $CDCl_3$): δ = 61.06 (d, J = 47.1 Hz, 3 P), 25.91 (q, J = 47.4 Hz, 1 P) ppm. Slow diffusion evaporation of hexane to a dichloromethane solution of [NiCl**L1^H**]$_2$[$NiCl_4$] resulted in the formation of crystals suitable for X-ray diffraction analysis. Mass Analysis (CS-ESI) [NiCl**L1^H**-H]$^+$: found: 1066.2097 calcd.: 1066.2075; negative: no fragments belonging to the complex could be observed. The NMR spectra of this compound are identical to [NiCl**L1^H**]BF_4.

[Ni(Cl)L1^H]BF$_4$ (2b): Compound **L1^H** (94.9 mg; 0.097 mmol; 1.0 equiv.), $NaBF_4$ (10.7 mg; 0.097 mmol; 1.0 equiv.) and $NiCl_2$·$6H_2O$ (23.1 mg; 0.097 mmol; 1.0 equiv.) were suspended in THF (10 mL) and stirred overnight. The green precipitate was filtered off, washed with Et_2O and was dried in vacuo yielding the complex as a green solid. Yield: 98.9 mg (0.086 mmol, 87.9 %) ^1H NMR (300 MHz, $CDCl_3$): δ = 7.81 (d, J = 8.1 Hz, 3 H), 7.27–7.17 (m, 9 H), 7.12–6.82 (m, 29 H), 6.29 (d, J = 8.5 Hz, 3 H), 2.67 (s, 9 H) ppm. ^{31}P NMR (121 MHz, $CDCl_3$): δ = 61.06 (d, J = 47.1 Hz, 3 P), 25.91 (q, J = 47.4 Hz, 1 P) ppm. $^{13}C\{^1H,^{31}P\}$ NMR (75 MHz, $CDCl_3$): δ = 139.65 (m, C_q), 136.03 (m, C_q), 130.94 (s, CH-ph), 130.02 (m, CH-ph), 128.99 (m, CH-ph), 126.99 (s, CH-ind), 123.57 (s, CH-ind), 122.27 (s, CH-ind), 115.78 (s, CH-ind), 10.69 (s, CH_3) ppm. Mass Analysis (CS-ESI) [NiCl**L1^H**-H]$^+$: found: 1066.2097 calcd.: 1066.2075; BF_4^-: found: 87.0049, calcd.: 87.0029.

[Fe(Cl)L1^H]BF$_4$ (3): Compound **L1^H** (1.05 g; 1.08 mmol; 1.0 equiv.), $NaBF_4$ (150 mg; 1.18 mmol; 1.1 equiv.) and $FeCl_2$ (118 mg; 1.08 mmol; 1.0 equiv.) were suspended in THF (40 mL) and stirred overnight. The purple reaction mixture was evaporated in vacuo and extracted with CH_2Cl_2 (100 mL). The purple solution was filtered, evaporated in vacuo, dissolved in THF (3 × 10 mL) and the solvents evaporated to dryness to remove the residual CH_2Cl_2. The solid was washed with Et_2O (3 × 5 mL) and dried in vacuo yielding the complex as a purple solid. Yield: 404.2 mg (35 %) ± half of the amount of solid was lost during the work up. Crystals suitable for X-ray diffraction analysis were obtained by layering a dichloromethane solution of FeCl**L1^H**BF_4 with pentane. ^1H NMR (300 MHz, $CDCl_3$): δ = 16.24 (bs), 14.74 (bs), 8.87 (bs), 8.35 (bs), 3.13 (bs), –0.37 (bs), –8.30 (bs), –9.14 (bs) ppm. UV/Vis (THF) λ_{max}: 553 nm^{-1}. Mass Analysis (CSI) [Fe(Cl)**L1^H**-H]$^+$: found: 1064.2105 calcd.: 1064.2073; BF_4^-: found: 87.0000, calcd.: 87.0029.

[Fe(Cl)L3^{iPr}]$_2$(BF$_4$)$_y$[FeCl$_4$]$_z$ (7): Compound **L3^{iPr}** (0.523 g; 0.68 mmol; 1.0 equiv.), $NaBF_4$ (0.082 g; 0.74 mmol; 1.1 equiv.) and $FeCl_2$ (0.178 g; 1.36 mmol; 2.1 equiv.) were suspended in THF (10 mL) and stirred for three days. The reaction mixture was evaporated to dryness, washed with pentane (5 × 10 mL) and extracted with CH_2Cl_2 (100 mL). The purple solution was filtered, evaporated in vacuo, dissolved in THF (3 × 10 mL) and evaporated in vacuo to remove the residual CH_2Cl_2. After washing with Et_2O and drying in vacuo the solid was obtained as a paramagnetic purple powder. Yield: not determined. Crystals were prepared by layering a dichloromethane solution with pentane at 5 °C. CSI mass analysis showed that the product was a mixture of [Fe(Cl)**L3^{iPr}**]$_x$(BF_4)$_y$-[$FeCl_4$]$_z$, but the exact ratio could not be determined. Mass Analysis (CSI) [Fe(Cl)**L3^{iPr}**]$^+$: found: 860.2963 calcd.: 860.3012. BF_4^-: found: 87.0049; [$FeCl_3$]$^-$: found: 160.8455; [$FeCl_4$]$^-$: 197.8139.

Reactions of **L1^{OMe}**, **L1^{CF3}** and **L2^H** with $FeCl_2$ were performed in a similar way as [Fe(Cl)**L3^{iPr}**]$_2$(BF_4)$_y$[$FeCl_4$]$_z$ leading to complexes **4**, **5**, **6** and **7** as mixtures of the [Fe(Cl)**L**]$^+$ with unknown amounts of BF_4 and $FeCl_4$. These mixtures were used as such for the reduction to the FeN_2**L** complex and the in situ analysis of the N_2 stretch frequency using infrared spectroscopy.

Reaction of L1^H with Fe(BF$_4$)$_2$: Compound **L1^H** (488 mg, 0.5 mmol) and $Fe(BF_4)_2$·$6H_2O$ (168 mg, 0.5 mmol) were suspended in 20 mL 1:1 (v/v) THF/toluene and heated at 70 °C for three days. The purple precipitated complex was filtered off and dried in vacuo to yield 369.2 mg of a purple solid. When the purple solid was dissolved in acetonitrile, a color change to orange was observed, yielding [$Fe(MeCN)_2$**L1^H**](BF_4)$_2$.

[Fe(MeCN)$_2$L1^H](BF$_4$)$_2$ (8): A solution of the purple powder obtained in the previous procedure in acetonitrile was set for crystallization by slow diffusion evaporation of methanol at 5 °C resulting in the formation of crystals suitable for X-ray diffraction analysis. ^{1}H NMR (300 MHz, CD_3CN): δ = broad peaks as a result of paramagnetic impurities: 7.80, 7.42, 7.39, 7.16, 6.85, 6.57, 6.37, 5.92, 3.00, 2.70, 2.60, 1.93. ^{31}P NMR (121 MHz, CD_3CN): δ = 116.77 (q), 97.59 (t, J = 44.2 Hz), 56.18 (q) ppm. The ^{13}C-NMR spectrum could not be obtained in pure form. ^{19}F NMR (282 MHz, CD_3CN): δ = 151.10 ppm. Mass analysis (CSI) [Fe**L1^H**-H]$^{2+}$: found: 514.6169, calcd.: 514.6192; [Fe**L1^H**]$^+$: found: 1048.2362 calcd.: 1048.2369; BF_4^-: found: 87.0049, calcd.: 87.0029.

Standard Procedure for the Reduction of the Complexes with KC$_8$: 20 mg of the complex was suspended with 2–5 equiv. of KC_8 in 2 mL of THF in the glovebox and stirred for 2–3 h. The solution was filtered and part of the solution was used for in situ infrared spectroscopy, the rest of the solution was set for crystallization by evaporation of pentane vapors to the THF solution. Crystals suitable for X-ray diffraction analysis formed for complexes FeCl**L1^H** (**14**), FeCl**L2^H** (**15**), FeCl**L3^{iPr}** (**16**) and FeN$_2$**L1^H** (**9**). Crystals of FeN$_2$**L1^H** (**9**) were obtained by layering of the THF solution with pentane.

CCDC 1579207 (for **1a**), 1579208 (for **2a**), 1579209 (for **3b**), 1579210 (for **7**), 1579211 (for **8**), 1579212 (for **14**), 1579213 (for **15**), 1579214 (for **16**), and 1579215 (for **9**) contain the supplementary crystallographic data for this paper. These data can be obtained free of charge from The Cambridge Crystallographic Data Centre.

Acknowledgments

We thank the National Research School Combination Catalysis (NRSC-C) and the Netherlands Organization for Scientific Research (NWO-CW) for a VENI grant 722.013.002 to W. I. D., and the University of Amsterdam (RPA Sustainable Chemistry) for funding. We thank Jan Meine Ernsting for assistance with NMR spectroscopy and Ed Zuidinga for mass spectrometry measurements.

Keywords: Iron · Cobalt · Nickel · Dinitrogen complexes · P ligands

[1] B. Su, Z.-C. Cao, Z.-J. Shi, *Acc. Chem. Res.* **2015**, *48*, 886–896.
[2] Y.-Y. Li, S.-L. Yu, W.-Y. Shen, J.-X. Gao, *Acc. Chem. Res.* **2015**, *48*, 2587–98.
[3] J. H. Docherty, J. Peng, A. P. Dominey, S. P. Thomas, *Nat. Chem.* **2016**, *8*, 1–6.
[4] I. Bauer, H.-J. Knölker, *Chem. Rev.* **2015**, *115*, 3170–3387.
[5] G. Wienhöfer, F. A. Westerhaus, K. Junge, M. J. Beller, *J. Organomet. Chem.* **2013**, *744*, 156–159.
[6] G. Wienhöfer, F. A. Westerhaus, K. Junge, R. Ludwig, M. Beller, *Chem. Eur. J.* **2013**, *19*, 7701.
[7] T. J. Korstanje, J. I. van der Vlugt, C. J. Elsevier, B. de Bruin, *Science* **2015**, *350*, 298–302.
[8] S. A. Burgess, K. Grubel, A. M. Appel, E. S. Wiedner, J. C. Linehan, *Inorg. Chem.* **2017**, *56*, 8580–8589.
[9] H. Fong, J. C. Peters, *Inorg. Chem.* **2015**, *54*, 5124–5135.
[10] C. Federsel, A. Boddien, R. Jackstell, R. Jennerjahn, P. J. Dyson, R. Scopelliti, G. Laurenczy, M. Beller, *Angew. Chem. Int. Ed.* **2010**, *49*, 9777; *Angew. Chem.* **2010**, *122*, 9971.
[11] C. Ziebart, C. Federsel, P. Anbarasan, R. Jackstell, W. Baumann, A. Spannenberg, M. Beller, *J. Am. Chem. Soc.* **2012**, *134*, 20701.
[12] J. L. Drake, C. M. Manna, J. A. Byers, *Organometallics* **2013**, *32*, 6891.
[13] C. Federsel, C. Ziebart, R. Jackstell, W. Baumann, M. Beller, *Chem. Eur. J.* **2012**, *18*, 72–75.
[14] F. Bertini, I. Mellone, A. Ienco, M. Peruzzini, L. Gonsalvi, *ACS Catal.* **2015**, *5*, 1254–1265.
[15] T. J. Del Castillo, N. B. Thompson, J. C. Peters, *J. Am. Chem. Soc.* **2016**, *138*, 5341–5350.
[16] R. B. Siedschlag, V. Bernales, K. D. Vogiatzis, N. Planas, L. J. Clouston, E. Bill, L. Gagliardi, C. C. Lu, *J. Am. Chem. Soc.* **2015**, *137*, 4638–4641.
[17] W. H. Wang, Y. Himeda, J. T. Muckerman, G. F. Manbeck, E. Fujita, *Chem. Rev.* **2015**, *115*, 12936–12973.
[18] S. Kuriyama, Y. Nishibayashi, "Catalytic Transformations of Molecular Dinitrogen by Iron and Cobalt–Dinitrogen Complexes as Catalysts" in *Nitrogen Fixation. Topics in Organometallic Chemistry, Vol. 60* (Ed.: Y. Nishibayashi), Springer, Cham, **2017**.
[19] L. D. Field, R. W. Guest, K. Q. Vuong, S. J. Dalgarno, P. Jensen, *Inorg. Chem.* **2009**, *48*, 2246–2253.
[20] D. Pennon, I. O. Koshevoy, F. Estevan, M. Sanaú, M. A. Ubeda, J. Pérez-Prieto, *Organometallics* **2010**, *29*, 703–706.
[21] J. Wassenaar, B. de Bruin, M. A. Siegler, A. L. Spek, J. N. H. Reek, J. I. van der Vlugt, *Chem. Commun.* **2010**, *46*, 1232–1234.
[22] J. Wassenaar, M. A. Siegler, A. L. Spek, B. De Bruin, J. N. H. Reek, J. I. van der Vlugt, *Inorg. Chem.* **2010**, *49*, 6495–6508.
[23] F. F. van der Watering, J. I. van der Vlugt, W. I. Dzik, B. de Bruin, J. N. H. Reek, *Chem. Eur. J.* **2017**, *23*, 12709–12713.
[24] F. F. van der Watering, N. Heijtbrink, J. I. van der Vlugt, W. I. Dzik, B. De Bruin, J. N. H. Reek, *Inorganics* **2017**, *5*, 73.
[25] L. Sacconi, *Coord. Chem. Rev.* **1972**, *8*, 351–367.
[26] J.-C. Hierso, R. Amardeil, E. Bentabet, R. Broussier, B. Gautheron, P. Meunier, P. Kalck, E. N. Supe, *Coord. Chem. Rev.* **2003**, *236*, 143–206.
[27] P. Stoppioni, F. Mani, L. Sacconi, *Inorg. Chim. Acta* **1974**, *11*, 227–230.
[28] L. Sacconi, M. Di Vaira, *Inorg. Chem.* **1978**, *17*, 810–815.
[29] W. H. Hohman, D. J. Kountz, D. W. Meek, *Inorg. Chem.* **1986**, *25*, 616–623.
[30] C. Bianchini, M. Peuzzini, A. Ceccanti, F. Laschi, P. Zanello, *Inorg. Chim. Acta* **1997**, *259*, 61–70.
[31] F. Mani, L. Sacconi, *Comments Inorg. Chem.* **1983**, *2*, 157–186.
[32] N. M. Kolyadina, V. I. Sokol, V. B. Kvartalov, V. V. Davydov, E. A. Fomicheva, A. T. Soldatenkov, V. S. Sergienko, *Russ. J. Inorg. Chem.* **2013**, *58*, 671–677.
[33] F. Oddon, E. Girgenti, C. Lebrun, C. Marchi-Delapierre, J. Pécaut, S. Ménage, *Eur. J. Inorg. Chem.* **2012**, 85–96.
[34] B. Xu, A. Ma, T. Jia, Z. Hao, W. Gao, Y. Mu, *Dalton Trans.* **2016**, *45*, 17966–17973.
[35] F. M. T. Almeida, M. F. N. N. Carvalho, A. M. Galvão, J. Cermák, V. Blechta, A. J. L. Pombeiro, B. L. Shaw, *Inorg. Chim. Acta* **2002**, *338*, 201–209.
[36] R. Langer, F. Bönisch, L. Maser, C. Pietzonka, L. Vondung, T. P. Zimmermann, *Eur. J. Inorg. Chem.* **2015**, *2015*, 141–148.
[37] B. J. Barrett, V. M. Iluc, *Organometallics* **2014**, *33*, 2565–2574.
[38] E. Angelescu, R. Ionescu, O. D. Pavel, R. Zăvoianu, R. Bîrjega, C. R. Luculescu, M. Florea, R. Olar, *J. Mol. Catal. A* **2010**, *315*, 178–186.
[39] A. Petuker, K. Merz, C. Merten, U. P. Apfel, *Inorg. Chem.* **2016**, *55*, 1183–1191.
[40] C. Fliedel, V. Rosa, B. Vileno, N. Parizel, S. Choua, C. Gourlaouen, P. Rosa, P. Turek, P. Braunstein, *Inorg. Chem.* **2016**, *55*, 4183–4198.
[41] A. W. Addison, T. N. Rao, J. Reedijk, J. van Rijn, G. C. Verschoor, *J. Chem. Soc., Dalton Trans.* **1984**, 1349–1356.
[42] T. Whyte, A. T. Casey, G. A. Williams, *Inorg. Chem.* **1995**, *34*, 2781–2787.
[43] C. Gendy, D. Spasyuk, A. Harrison, R. Roesler, *Inorg. Chim. Acta* **2017**, https://doi.org/:10.1016/j. ica.2017.10.017.
[44] The DFT [BP86, SV(P)] calculated energy of the pentet state (HS) and the singlet state (LS) are higher in energy than the triplet state (IS) by 24 kcal/mol and 7.7 kcal/mol respectively.
[45] R. B. King, R. N. Kapoor, M. S. Saran, P. Kapoor, *Inorg. Chem.* **1971**, *10*, 1851–1860.
[46] G. Jia, S. D. Drouin, P. G. Jessop, A. J. Lough, R. H. Morris, *Organometallics* **1993**, *12*, 906–916.
[47] J. O. Yu, C. S. Browning, D. H. Farrar, *Chem. Commun.* **2008**, 1020–1022.
[48] D. L. Dubois, A. Miedaner, *Inorg. Chem.* **1986**, *25*, 4642–4650.
[49] S. Hinrichsen, A.-C. Schnoor, K. Grund, B. Flöser, A. Schlimm, C. Näther, J. Krahmer, F. Tuczek, *Dalton Trans.* **2016**, *45*, 14801–14813.
[50] T. A. George, D. J. Rose, Y. Chang, Q. Chen, J. Zubieta, *Inorg. Chem.* **1995**, *34*, 1295–1298.

[51] N. P. Mankad, M. T. Whited, J. C. Peters, *Angew. Chem. Int. Ed.* **2007**, *46*, 5768–5771; *Angew. Chem.* **2007**, *119*, 5870.
[52] M. E. Moret, J. C. Peters, *Angew. Chem. Int. Ed.* **2011**, *50*, 2063–2067; *Angew. Chem.* **2011**, *123*, 2111.
[53] S. E. Creutz, J. C. Peters, *J. Am. Chem. Soc.* **2014**, *136*, 1105–1115.
[54] I. S. Weitz, M. Rabinovitz, *J. Chem. Soc., Perkin Trans. 1* **1993**, 117–120.
[55] Bruker, *SAINT-Plus*, Bruker AXS Inc., Madison, Wisconsin, USA, **2001**.
[56] G. M. Sheldrick, *SADABS and TWINABS*, University of Göttingen, Germany, **2008**.
[57] G. M. Sheldrick, *SHELXT*, University of Göttingen, Germany, **2012**.
[58] G. M. Sheldrick, *Acta Crystallogr., Sect. A* **2015**, *71*, 3–8.
[59] A. L. Spek, *Acta Crystallogr., Sect. D* **2009**, *65*, 148–155.

Received: October 16, 2017